Lattice Boltzmann algorithm for continuum multicomponent flow

I. Halliday, A. P. Hollis, and C. M. Care
Materials and Engineering Research Institute, Sheffield Hallam University, Sheffield, Howard Street, S1 1WB, United Kingdom
(Received 30 January 2007; revised manuscript received 30 May 2007; published 31 August 2007)

We present a multicomponent lattice Boltzmann simulation for continuum fluid mechanics, paying particular attention to the component segregation part of the underlying algorithm. In the principal result of this paper, the dynamics of a component index, or phase field, is obtained for a segregation method after U. D'Ortona *et al.* [Phys. Rev. E **51**, 3718 (1995)], due to Latva-Kokko and Rothman [Phys. Rev. E **71** 056702 (2005)]. The said dynamics accord with a simulation designed to address multicomponent flow in the continuum approximation and underwrite improved simulation performance in two main ways: (i) by reducing the interfacial microcurrent activity considerably and (ii) by facilitating simulational access to regimes of flow with a low capillary number and drop Reynolds number [I. Halliday, R. Law, C. M. Care, and A. Hollis, Phys. Rev. E **73**, 056708 (2006)]. The component segregation method studied, used in conjunction with Lishchuk's method [S. V. Lishchuk, C. M. Care, and I. Halliday, Phys. Rev. E **67**, 036701 (2003)], produces an interface, which is distributed in terms of its component index; however, the hydrodynamic boundary conditions which emerge are shown to support the notion of a sharp, unstructured, continuum interface.

DOI: 10.1103/PhysRevE.76.026708 PACS number(s): 47.11.−j, 05.20.Dd, 51.10.+y

I. INTRODUCTION

The simulation of multicomponent fluids at a low Reynolds number and low capillary number is of interest in a variety of important applications. However, for many, such simulations have been prohibitively demanding from a computational point of view. The relatively recent advent of multicomponent lattice Boltzmann (lB) schemes have done much to improve matters [1].

A variety of multicomponent flows on a range of length and time scales are conveniently modeled using the multicomponent lB method (see below); the work presented here is of most relevance to applications of which the recent microfluidic flow simulations of Dupin *et al.* [2] are an example. Such flows as are addressed in Ref. [2] are formally characterized as complex, incompressible flows at a small Reynolds number Re and small capillary number Ca. Multiple blood cells in venule-scale flows have also been represented in this regime, with lB [3,4]. Improving simulations of such non-Brownian colloids, addressed in the continuum fluid approximation, where fluid-fluid interfaces have no assumed structure and appear as boundary conditions, are the object of this work.

The several multicomponent lB methods may be distinguished by the different ways in which they impose a fluid-fluid interface [5–9]. See also Ref. [1] for a survey of the methods' relative advantages and applications. In problems where the kinematics of phase separation feature, Swift's method [5,7], based as it is upon Cahn-Hilliard theory, represents an appropriate choice of lB interface algorithm. Here we aim to address only completely immiscible mixtures in a continuum approximation. For such applications, physical accuracy, efficiency, and simplicity have often encouraged the choice of an lB interface algorithm of a type pioneered by Gunstensen *et al.* [8] and later modified by Lishchuk [9]. Details of a modified form of Lishchuk's method, which takes account of the work of Guo [10] may be found in Ref. [11].

In Lishchuk's method the interface is based on the continuum level stress boundary conditions, which apply on an unstructured interface between completely separated fluids [12]; it produces narrow interfaces with reduced microcurrents (or "spurious velocities" [1]), it has an independently adjustable interfacial tension, and it sustains interfacial tensions larger than Gunstensen's method [8].

Despite some successes [2], continuum multicomponent lB (with Lishchuk's method or Gunstensen's method) encounters a problem reaching a low Ca and drop Reynolds number Re_d; as Ca and Re_d both decrease there is an increasing tendency for suspended drops of immiscible fluid to facet and to attach, or *pin* to the simulation lattice in an effective loss of Galilean invariance [11]; here we address this problem together with the related problem of the interfacial microcurrent [11].

In this paper we draw attention to one element of the multicomponent lB algorithm, which will impact on its uptake; an elegant, efficient alternative fluid-fluid segregation process, devised by d'Ortona *et al.* [13]. We are certainly not the first to recognize its utility. Recently, Latva-Kokko and Rothman have demonstrated the advantages of a segregation method closely related to d'Ortona's in respect of an almost eliminated tendency to drop pinning [14]. Concentrating on application to the continuum regime, where drop evaporation must be completely interrupted, we show that, by adopting the approach of d'Ortona and Latva-Kokko that (i) the interfacial microcurrent is, likewise, almost eliminated and (ii) the kinematics of the interface may be predicted. What emerges is a simple, relatively efficient, analytic algorithm with determinate phase-field dynamics, very low microcurrent activity, very low pinning, and high adaptability in the continuum approximation.

Our paper is set out as follows. In Sec. II we set out the background lB model. In Sec. III we analyze the segregation method of d'Ortona *et al.* from the perspective of continuum hydrodynamics. In Sec. IV we present results in support of the observations made in Sec. III and the appendixes. Useful

but noncentral results are, for clarity, placed in the Appendixes of Sec. 6.

II. MULTICOMPONENT LATTICE BOLTZMANN IN THE CONTINUUM APPROXIMATION

The work reported here and in Ref. [9] is based upon the popular single component, isothermal, single relaxation time lB variant widely designated the lattice Bhatnagar-Gross-Krook (LBGK) model, due to Qian *et al.* [15]. The LBGK model is expressed in terms of an evolution (collision and subsequent propagation) equation for a discretized single-particle momentum distribution function f_i [1]; to this evolution a source term $\phi_i(\mathbf{r})$ may be added as follows:

$$f_i(\mathbf{r}+\mathbf{c}_i,t+1)=f_i(\mathbf{r},t)-\omega[f_i(\mathbf{r},t)-f_i^{(0)}(\rho,\rho\mathbf{u})]+\phi_i(\mathbf{r}). \tag{1}$$

The source term ϕ_i in Eq. (1) has the effect of impressing a body force in the fluid, which emerges from this kinetic (f_i-based) description; $0\leq\omega\leq 2$ is the single selectable parameter which, with LBGK, controls the viscosity of the fluid [1]; all other symbols have their usual meaning. Below we discuss how source term ϕ_i inserts a body force of limited range to produce an interfacial pressure step in the fluid. Note, Eq. (1) assumes unit time step.

From the single-particle momentum distribution function f_i governed by Eq. (1), and its appropriately chosen, isothermal equilibrium contribution $f_i^{(0)}(\rho,\rho\mathbf{u})$, hydrodynamic observables ρ and $\mathbf{u}$ emerge [1] as follows:

$$\rho(\mathbf{r},t)\equiv\sum_i f_i(\mathbf{r},t)=\sum_i f_i^{(0)}(\rho,\rho\mathbf{u}), \tag{2}$$

$$\mathbf{u}(\mathbf{r},t)\equiv\frac{1}{\rho}\sum_i f_i(\mathbf{r},t)\mathbf{c}_i=\frac{1}{\rho}\sum_i f_i^{(0)}(\rho,\rho\mathbf{u})\mathbf{c}_i. \tag{3}$$

For the most appropriate definition of equilibrium $f_i^{(0)}(\rho,\rho\mathbf{u})$, see Ref. [17].

For a constant source term ϕ_i, Chapman-Enskog analysis [1] may be used to derive lB's characteristic weakly compressible form of the incompressible Navier-Stokes equations, now with a body force. For example, the choice

$$\phi_i=t_p\frac{1}{k_2}\mathbf{F}\cdot\mathbf{c}_i, \tag{4}$$

represents one, simple, widely used device for inserting a uniform body force (or uniform pressure gradient) $\mathbf{F}$ into the lattice Navier-Stokes equations

$$\frac{\partial}{\partial t}\rho u_\alpha+\frac{\partial}{\partial x_\beta}\rho u_\beta u_\alpha=-\frac{\partial}{\partial x_\alpha}c_s^2\rho+\frac{\partial}{\partial x_\beta}(2\rho\nu S_{\alpha\beta})+F_\alpha, \tag{5}$$

where kinematic viscosity $\nu\equiv\frac{1}{6}\left(\frac{2}{\omega}-1\right)$ and $S_{\alpha\beta}$ is the strain rate tensor; the lattice-dependent constant k_2 and the link weights t_p are discussed at the beginning of Sec. III. We note that, throughout, (i) Greek *subscripts* denote Cartesian vector components x, y, etc., and (ii) the summation convention applies only to repeated Greek subscripts.

The precise relationship between the fluid body force and the source term ϕ_i is an issue throughout this work. A constant microscopic source term ϕ_i in Eq. (1), and the resulting macroscopic body force, in Eq. (5), are related as follows:

$$\mathbf{F}=k_2\sum_i\phi_i\mathbf{c}_i. \tag{6}$$

For present purposes, however, the body force has spatial variation: $\mathbf{F}\rightarrow\mathbf{F}(\mathbf{r})$ [11], which necessitates spatial variation in $\phi_i(\mathbf{r})$; as Guo *et al.* point out [10], such a generalization complicates the derivation of Eq. (5) above and requires (i) a more complicated relationship between $\mathbf{F}(\mathbf{r})$ and $\phi_i(\mathbf{r})$ than that given for Eq. (6) and (ii) a redefinition of $\mathbf{u}$. Before we state a modified relationship, it will be useful to consider the form of fluid interface force, which ϕ_i should generate, and where this force should be applied.

Fluid-fluid interface dynamics are applied in regions of the lattice where two immiscible fluids interact (and segregate). The two fluids concerned are designated red and blue. The momentum distribution function f_i is now specified for these red and blue fluids individually. We take

$$f_i(\mathbf{r},t)=R_i(\mathbf{r},t)+B_i(\mathbf{r},t), \tag{7}$$

with the nodal density of red and blue fluids now defined in individual, conserved quantities as follows:

$$R(\mathbf{r},t)\equiv\sum_i R_i(\mathbf{r},t),\quad B(\mathbf{r},t)\equiv\sum_i B_i(\mathbf{r},t). \tag{8}$$

Note, however, that Eqs. (2) and (3) remain valid; the velocity of the single *sum* lattice fluid is still defined by Eq. (3).

As different fluids mix in an interfacial region they define a single mixture, or sum, fluid which is evolved according to evolution Eq. (1), the interface dynamics being captured by the source term ϕ. The mixture is then segregated. Segregation is not a passive process; the way in which it is achieved influences the physical accuracy of the model. We will present an analysis of a particular, advantageous, segregation method in Sec. III; in the remainder of this section we consider salient detail of the interface force and corresponding source term.

To identify mixed fluid, first distinguish between individual lattice fluids themselves. Our multicomponent lB uses a phase field based upon the densities of "red" and "blue" fluids present at a node. Following the notation of [9], we define a fluid component index, or phase field $\rho^N(\mathbf{r})$ as follows:

$$\rho^N(\mathbf{r},t)\equiv\left(\frac{R(\mathbf{r},t)-B(\mathbf{r},t)}{R(\mathbf{r},t)+B(\mathbf{r},t)}\right),\quad -1\leq\rho^N(\mathbf{r})\leq 1. \tag{9}$$

Red and blue fluids mix under the lB propagation step [1] defining an interfacial region; here an additional force is applied to the sum fluid capturing the effects of interfacial tension. The two fluids are segregated numerically [8] or by the method of Sec. III. Whatever the segregation algorithm used, in Lishchuk's lB interface method [9] a surface tension inducing interface, force $\mathbf{F}(\mathbf{r})$, is defined in terms of the gradient of $\rho^N(\mathbf{r})$. To achieve a cross-interfacial pressure step pro-

portional only to K, the local curvature in the ρ^N field, use a fluid body force as follows:

$$\mathbf{F}(\mathbf{r}) \equiv -\frac{1}{2}\alpha K \nabla \rho^N, \tag{10}$$

with α a surface tension parameter. Note, the right-hand side of Eq. (10) vanishes for constant ρ^N. Using the negative of a normalized phase-field gradient as the interface normal $\hat{\mathbf{n}}$, K is obtained from the surface gradient as follows:

$$K = n_x n_y \left(\frac{\partial}{\partial y} n_x + \frac{\partial}{\partial x} n_y \right) - n_x^2 \frac{\partial}{\partial y} n_y - n_y^2 \frac{\partial}{\partial x} n_x, \tag{11}$$

where [11]

$$\hat{\mathbf{n}} \equiv -\frac{\mathbf{f}'}{|\mathbf{f}'|}, \qquad \mathbf{f}' \equiv \nabla \rho^N. \tag{12}$$

It is appropriate to emphasize here that all the gradients are calculated numerically using suitable finite differences [11]; a source of significant computational overhead. We shall consider the feasibility of appropriate, *locally calculated* alternatives in Sec. IV and in the Appendix C.

The cumulative effect of the force in Eq. (10) is to produce a pressure step across the interfacial region. Assuming K to vary slowly, the total local force perpendicular to a unit length of interface, which is numerically equal to the pressure step, is obtained from the integral of the force (density) $\mathbf{F}(\mathbf{r})$, between the terminal points P_R and P_B, of a short, normal path with element dn as follows:

$$\Delta P = \left| \int_{P_B}^{P_R} \mathbf{F} dn \right| = \frac{1}{2}\alpha K [\rho^N(P_R) - \rho^N(P_B)] = \alpha K, \tag{13}$$

where P_B and P_R are embedded in the blue and red fluids, respectively, so $\rho^N(P_R) = -\rho^N(P_B) = 1$.

The interface algorithm outlined in the current section is based upon a spatially and temporally varying force applied locally in what is a single fluid, to eliminate curvature in a phase field. This, it may be shown, accurately represents interface dynamics (stress conditions) [9]. However, the extent to which the kinematic condition of mutual impenetrability is implicit is unclear; the fact that there is a single "sum" fluid means that the combined momentum of the mixture of fluids is continuous across an interfacial region but the velocities of the red and blue fluids may not be easily defined close to the interface. We return to this point in a separate paper [19].

The methodology of Guo addresses the issue of a spatially varying body force in a progression of earlier work of, in particular, Verberg and Ladd [16]; it furnishes an expression for an appropriate source term ϕ_i in terms of *variable* macroscopic force $\mathbf{F}(\mathbf{r})$ [10] as follows:

$$\phi_i(\mathbf{r}) \equiv t_p \left(1 - \frac{\omega}{2} \right) [3(\mathbf{c}_i - \mathbf{u}^*) + 9(\mathbf{c}_i \cdot \mathbf{u}^*)\mathbf{c}_i] \cdot \mathbf{F}(\mathbf{r}), \tag{14}$$

where we emphasize the fluid velocity is redefined effectively to carry some of the influence of any external body force as follows:

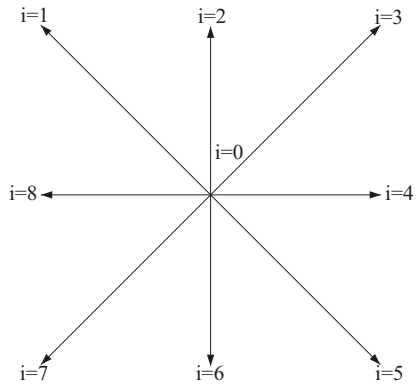

FIG. 1. The nodal velocity set and subscripting convention for the two-dimensional, nine velocity, D2Q9, lattice. Note that links classified with odd values of subscript i have a larger length. The weights corresponding to the links are listed in Table I.

$$\mathbf{u}^* \equiv \frac{1}{\rho} \left(\sum_i f_i \mathbf{c}_i + (1-f)\mathbf{F}(\mathbf{r}) \right), \quad f = \frac{1}{2}. \tag{15}$$

We shall return to this point and the definition of link weights t_p in Sec. III. Note that Eq. (14) accounts for the case of a macroscopic force, which also contains time dependence. Of course, in a standard LBGK model, $f=1$ in definition (15). It is worth the inconvenience of retaining the parameter f, introduced above, as it is possible easily to adapt our key results to a standard LBGK model simply by changing its value to $f=1$.

With Guo's methodology [10], the model's Navier-Stokes equation (5) now acquires position dependence in the body-force term as follows:

$$\frac{\partial}{\partial t}\rho u_\alpha^* + \frac{\partial}{\partial x_\beta}\rho u_\beta^* u_\alpha^* = -\frac{\partial}{\partial x_\alpha}(c_s^2 \rho) + \frac{\partial}{\partial x_\beta}(2\rho\nu S_{\alpha\beta}^*) + F_\alpha(\mathbf{r}). \tag{16}$$

We emphasize that $F_\alpha(\mathbf{r})$ should be regarded as that interface force defined in Eq. (10).

III. ANALYSIS OF SEGREGATION RULE

Recall, R (B) denotes the density of red (blue) fluid present at the node, position $\mathbf{r}$. In terms of phase-field parameter ρ^N, these quantities are

$$R(\mathbf{r},t) = \frac{1}{2}\rho(\mathbf{r},t)[1 + \rho^N(\mathbf{r},t)], \tag{17}$$

$$B(\mathbf{r},t) = \frac{1}{2}\rho(\mathbf{r},t)[1 - \rho^N(\mathbf{r},t)]. \tag{18}$$

For definiteness and simplicity we shall consider the D2Q9 lattice defined in Fig. 1. However, results will generalize to D3QN transparently, for lattice and model dimensionality enter only through parameter k_2, which is retained explicitly throughout. We shall use unit time step and lattice spacing for the same reasons. Whether in two or three di-

TABLE I. The link weights t_p and indexing for the D2Q9 lattice depicted in Fig. 1.

i	0	Even	Odd
$\lvert\mathbf{c}_i\rvert$	0	1	$\sqrt{2}$
t_p	4/9	1/9	1/36

mensions, all lattices are considered to have the usual isotropy properties as follows:

$$\sum_i t_p c_{i\alpha} c_{i\beta} = k_2 \delta_{\alpha\beta}, \tag{19}$$

$$\sum_i t_p c_{i\alpha} c_{i\beta} c_{i\gamma} c_{i\delta} = k_4 (\delta_{\alpha\beta}\delta_{\gamma\delta} + \delta_{\alpha\gamma}\delta_{\beta\delta} + \delta_{\alpha\delta}\delta_{\beta\gamma}), \tag{20}$$

odd moments of the lattice basis vectors $\mathbf{c}_i$ being zero. In Eqs. (19) and (20) the link weights t_p are a set of scalar quantities, which weight the directions of the lattice according to the length of velocity vector $\mathbf{c}_i$. The values of t_p and $\mathbf{c}_i$ for the case of the D2Q9 LBGK lattice are defined in Table I. Note that, for the D2Q9 lattice $k_2 = \frac{1}{3}$.

Component segregation is achieved by allocating color density R (say) to the sum fluid's momentum distribution function f_i optimally at each node [8]. It is the purpose of this section to demonstrate the advantages of, and to analyze, an alternative approach, after d'Ortona [13], due to Latva-Kokko and Rothman [14]. We shall adhere to the following convention. A postcollision, prepropagation momentum density is indicated by the use of a dagger superscript; accordingly, Eq. (1) becomes

$$f_i^\dagger(\mathbf{r},t) = f_i(\mathbf{r},t) - \omega[f_i(\mathbf{r},t) - f_i^{(0)}(\rho,\rho\mathbf{u}^*)] + \phi_i(\mathbf{r}), \tag{21}$$

in which the modified velocity is used to calculate the equilibrium. Note also that the postcollision momentum distribution function $f_i^\dagger$ includes the source contribution ϕ_i defined in Eq. (14).

For convenience, the collision process is subsequently resolved into two steps; first, that expressed above, and second, the segregation process. Postcollision, postsegregation (recolored) quantities will be indicated by the use of a double dagger superscript.

Before proceeding, it is necessary to remark on certain properties of the Guo's LBGK model [10]. As we have commented, the effect of a fluid body force is partly carried in a redefined velocity, which has a notable consequence for the first moment of the $f_i^\dagger$ as defined in Eq. (21) as follows:

$$\sum_i f^\dagger c_{i\alpha} = \rho u_\alpha^* + f F_\alpha, \quad f = \frac{1}{2}, \tag{22}$$

which result may be established by replacing f_i with $(f_i^{(0)} + \epsilon f_i^{(1)} + \cdots)$ in the moment of Eq. (21) with $c_{i\alpha}$, then substituting using Eqs. (5), (9a), and (17) of Guo *et al.* [10], with Guo's time-step parameter $\Delta t = 1$. It is well worth noting that, in the Guo model, in the absence of any local force $F_\alpha = \phi_i = 0$, (i) momentum is still conserved locally and (ii) the definition of velocity reverts to its usual form. For the usual LBGK model, the parameter f introduced in Eq. (22) would, of course, take the value $f = 1$.

A. Acceleration of the color flux

We define the postpropagation, precollision, nodal red and blue masses and single color fluxes in terms of the link-based quantities $R_i(\mathbf{r},t)$ and $B_i(\mathbf{r},t)$ as follows:

$$R(\mathbf{r},t) = \sum_i R_i(\mathbf{r},t), \quad B(\mathbf{r},t) = \sum_i B_i(\mathbf{r},t), \tag{23}$$

$$q_{R\alpha}(\mathbf{r},t) = \sum_i R_i(\mathbf{r},t) c_{i\alpha}, \quad q_{B\alpha}(\mathbf{r},t) = \sum_i B_i(\mathbf{r},t) c_{i\alpha}. \tag{24}$$

We also define an overall color flux as follows:

$$\mathbf{q}(\mathbf{r},t) \equiv \mathbf{q}_R(\mathbf{r},t) - \mathbf{q}_B(\mathbf{r},t), \tag{25}$$

which is further discussed in Appendix B.

We define a slightly modified color segregation after Latva-Kokko and Rothman's form of d'Ortona's segregation [14,13] as follows:

$$R_i^{\dagger\dagger} = \frac{R}{R+B} f_i^\dagger + \beta \frac{RB}{R+B} t_p \cos(\theta_f - \theta_i) |\mathbf{c_i}|, \tag{26}$$

$$B_i^{\dagger\dagger} = \frac{B}{R+B} f_i^\dagger - \beta \frac{RB}{R+B} t_p \cos(\theta_f - \theta_i) |\mathbf{c_i}|, \tag{27}$$

in which θ_f (θ_i) is the polar angle of the color field $\mathbf{f}'(\mathbf{r})$, (link) and $R_i^{\dagger\dagger}$ denotes the postcollision, postsegregation value of the momentum density of the red fluid associated with link i. The inclusion, in Eq. (26), of the factor $|\mathbf{c_i}|$ makes the resulting algorithm more amenable to analysis while preserving the essential ideas of Latva-Kokko and Rothman and d'Ortona *et al.* [14,13]. While our Eq. (26) essentially accords with Eq. (9) of Latva-Kokko and Rothman [14] (the latter being an improvement over the original method expressed in Eq. (8) of d'Ortona *et al.* [13]), it will be necessary to revisit certain of Latva-Kokko and Rothmans's results, in Sec. III B, where segregation parameter β is considered in more detail, and in Appendix A.

It is necessary to note two properties of Eq. (26). First,

$$\sum_i R_i^{\dagger\dagger} = \frac{R}{R+B} \sum_i f_i^\dagger = R, \tag{28}$$

where we have used the identity $\cos(\theta_f - \theta_i)|\mathbf{c}_i| = \cos(\theta_f) c_{ix} + \sin(\theta_f) c_{iy}$. Second,

$$\sum_i R_i^{\dagger\dagger} \mathbf{c}_i \equiv \mathbf{q}_R^{\dagger\dagger} = R\mathbf{u}^* + \beta k_2 \frac{RB}{R+B} \hat{\mathbf{f}}' + f \frac{R}{R+B} \mathbf{F}, \tag{29}$$

where we have used Eq. (22) and those properties of even lattice moments given in Eqs. (19) and (20), the unit vector $\hat{\mathbf{f}}'$ is defined in Eq. (12), $\mathbf{F}$ is any continuum body force and, recall

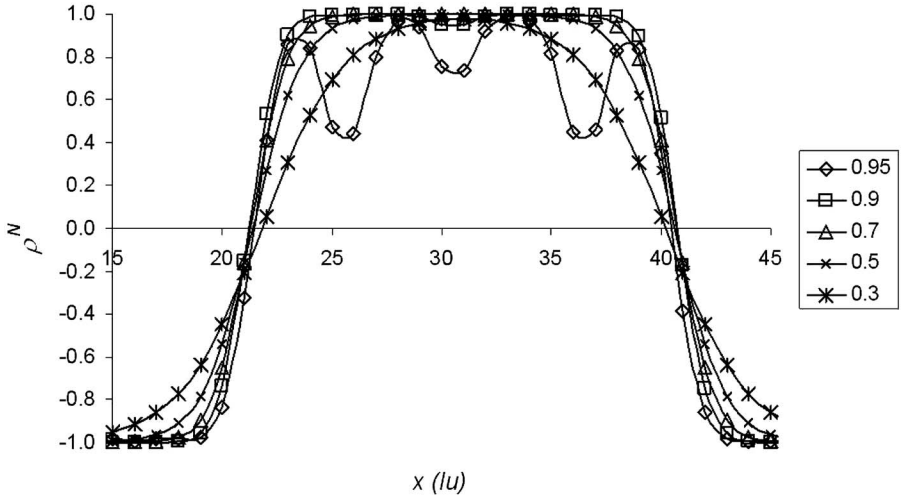

FIG. 2. Variation of the phase-field parameter ρ^N with distance x across the equator of a red ($\rho^N=1$) drop of approximate initial radius 10 lattice units, obtained for a range of segregation parameters β [Eq. (26) and figure key].

$$f=\frac{1}{2},1, \tag{30}$$

for Guo's LBGK model variant [10] and standard LBGK, respectively. For the D2Q9 lattice, $k_2=1/3$ (and $k_4=1/9$). For the segregation of blue let $\theta_f\rightarrow(\theta_f+\pi)$; hence, from Eq. (29), the net flux of the color vector

$$\mathbf{q}^{\dagger\dagger}\equiv\mathbf{q}_R^{\dagger\dagger}-\mathbf{q}_B^{\dagger\dagger}=\sum_i (R_i^{\dagger\dagger}\mathbf{c}_i-B_i^{\dagger\dagger}\mathbf{c}_i), \tag{31}$$

may be written as follows:

$$\mathbf{q}^{\dagger\dagger}=(R-B)\mathbf{u}^*+2\beta k_2\frac{RB}{R+B}(\cos(\theta_f),\sin(\theta_f))+f\rho^N\mathbf{F}, \tag{32}$$

and replacing quantities R and B, using Eqs. (17) and (18), Eq. (32) takes the form

$$\mathbf{q}^{\dagger\dagger}=\rho\rho^N\mathbf{u}^*+\frac{1}{2}\beta k_2\rho(1-\rho^{N2})\hat{\mathbf{f}}'+f\rho^N\mathbf{F}. \tag{33}$$

Now, $\mathbf{q}^{\dagger\dagger}=\rho\rho^N\mathbf{u}^*$ represents a postcollision color concentration advecting in flow. Neglecting for the moment correlations between $\mathbf{q}$ and $\mathbf{q}^{\dagger\dagger}$, the segregation expressed in Eq. (26) tends to *accelerate* the color flux in the direction of the color field at the rate $\frac{1}{2}\beta k_2\rho(1-\rho^{N2})$.

Now, in Appendix A, we consider a distributed, flat interface, centered on $x=x_0$, embedded in a rest fluid and obtain, by analytical methods, a solution for the steady-state spatial variation in the phase field as follows:

$$\rho^N=\tanh[k(x-x_0)],\quad k=\beta, \tag{34}$$

for two cases (i) the interface parallel to the short links of a D2Q9 lattice and (ii) the interface parallel to long links of a D2Q9 lattice. Furthermore, for a distributed, circular drop interface, with $0<\beta<0.7$, simulation results like those in Fig. 2 (which correspond to $\beta=0.7$, note) show that the steady interface profile generated using Eq. (26) is well approximated (see below) by a phase-field parameter variation as follows:

$$\rho^N(s)=\tanh(ks),\quad k=\beta, \tag{35}$$

in which s measures distance in the direction of $\hat{\mathbf{f}}'$ with $s=0$ corresponding to the center of the interface. Supported by these observations, we take in general,

$$\nabla\rho^N\approx k\,\mathrm{sech}^2(ks)\hat{\mathbf{f}}'=k(1-\rho^{N2})\hat{\mathbf{f}}',\quad k=\beta. \tag{36}$$

We shall, however, retain k as the interface parameter throughout our analysis, setting $k=\beta$ only in final results.

In fact, for the case of a D2Q9 lattice, solution (34) may be shown to describe interfacial orientations with the interface parallel to short lattice links (the case considered in Appendix A) and also with the interface parallel to the long lattice links; this demonstrates the isotropy implicit in the distributed interface and accords well with Latva-Kokko and Rothman's observations.

The color flux after the segregation between color components may be written as follows:

$$\mathbf{q}^{\dagger\dagger}=\rho\rho^N\mathbf{u}^*+\frac{1}{2}\frac{\beta}{k}k_2\rho\,\nabla\rho^N+f\rho^N\mathbf{F}. \tag{37}$$

The result expressed in Eqs. (33) and (37) generalizes straightforwardly into three dimensions as follows:

$$R_i^{\dagger\dagger}=\frac{R}{R+B}f_i^{\dagger}+\beta\frac{RB}{R+B}t_p\hat{\mathbf{f}}'\cdot\mathbf{c}_i. \tag{38}$$

B. Stability of a continuum interface

For application to the continuum hydrodynamic regime, it is necessary to impose limitations on the range of parameter β in Eq. (26). Figure 2 shows the variation of the phase field ρ^N across the equator of a stationary drop, initial radius 20 lattice units, for a range of *beta* values. Clearly, interfacial thickness decreases as β increases. However, for $\beta\gtrsim0.7$, there is no stable steady state. This is manifest in the data of Fig. 2 in *overjump* behavior which, for application to the continuum regime with arrested evaporation, represents an instability.

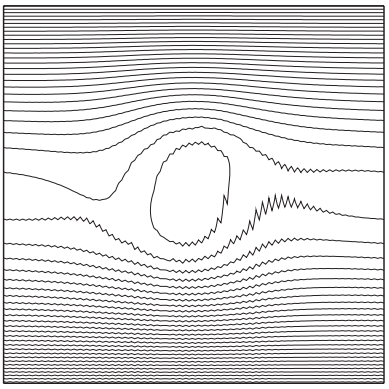

FIG. 3. Contours of constant value for the rectangular stream function obtained for a two-dimensional drop with numerical segregation, exposed to a small, symmetric shear flow.

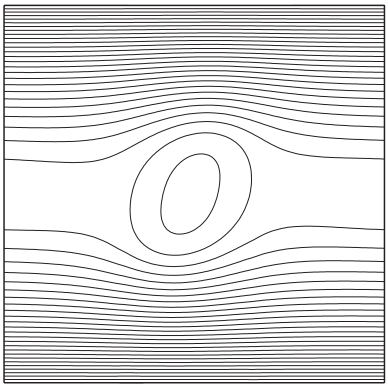

FIG. 4. Contours of constant value for the rectangular stream function obtained for a two-dimensional drop with the segregation method after D'Ortona [13], analyzed in Sec. III. Again the drop was exposed to a small, symmetric shear flow, identical to that used for the data of Fig. 3.

An approximate maximum stable value for segregation parameter β_{max} may be obtained from the condition $R_i^{\dagger\dagger} \leqslant f_i^{\dagger}$ and Eq. (38). We require

$$\frac{R}{R+B} f_i^{\dagger} + \beta \frac{RB}{R+B} t_p \hat{\mathbf{f}}' \cdot \mathbf{c}_i \leqslant f_i^{\dagger} \quad \forall\, i, \tag{39}$$

from which it is straightforward to obtain the inequality

$$t_p \beta R \hat{\mathbf{f}}' \cdot \mathbf{c}_i \leqslant f_i^{\dagger}. \tag{40}$$

The upper bound for β must correspond to a maximum of the scalar product $\hat{\mathbf{f}}' \cdot \mathbf{c}_i$; that is, when $\hat{\mathbf{f}}'$ is parallel to $\mathbf{c}_i$ for some particular link $i=I$, which we suppose to have longest possible length l_{max},

$$t_p \beta_{max} R l_{max} \leqslant f_I^{\dagger}. \tag{41}$$

Approximating $f_I^{\dagger} \approx f_I^{(0)}(\rho, \mathbf{0}) = t_p \rho$ and taking the maximum possible value of R (which is close to ρ) provides the required maximum stable value for β, consistent with arrested evaporation. For a D2Q9 lattice, $l_{max} = \sqrt{2}$, so, for our particular simulations,

$$\beta_{max} \lesssim \frac{1}{\sqrt{2}} = 0.71, \tag{42}$$

which value agrees very well indeed with simulations at low Re, Ca. It is important to note that the practical upper bound approximated in this way may be reduced in other regimes of more rapid multicomponent flow, when the f_is depart further from their equilibrium values.

Compared with the formulaic segregation expressed in Eq. (38), numerical segregation [8] produces much narrower interfaces; typically its phase field switches in ~1.5 lattice spacings [11]. An obvious question arises around replacing a numerical segregation by the formulaic segregation; while it is affected by pinning, and computationally it is much slower, surely the sharper interface of numerical segregation better accords with the continuum concept of a discontinuous interface? In fact, a close examination of the rectangular stream function of symmetrically sheared drops, maintained by numerical segregation (Fig. 3) and formulaic segregation (Fig. 4) provides a reply.

Figures 3 and 4 relate otherwise identical, slightly sheared drops maintained (respectively) by numerical segregation and formulaic segregation. The last open and first closed contours have been selected closely to *sandwich* the interface. In Fig. 3, this pair of contours exhibit oscillations of an amplitude which, when resolved in the direction of the local interface normal, extend over ≤5 lattice spacings exposing a noisy velocity field in the region of the interface. Such noise is absent from the equivalent results of Fig. 4. In fact, it is possible to examine the precise hydrodynamic boundary conditions recovered in this interfacial region and to develop, for formulaic segregation, simple, robust, highly adaptable and very effective algorithmic corrections, which effectively sharpen the interface [19]. Furthermore, even though the phase-field interface is sharper, the hydrodynamic interface obtained with numerical segregation (as defined by properties of the velocity field) is diffuse over a distance comparable to the phase-field variation obtained with formulaic segregation. So, with numerical segregation, the interface is not consistently sharper. It is appropriate also to emphasize that this problem only becomes more acute as drop surface tension (deformation) increases (decreases).

C. Dynamics of the phase field

The dynamics of numerical species segregation has not, to our knowledge, been derived. It is a considerable advantage that d'Ortona's formulaic method allows one to derive the dynamics of the phase field, which result from use of its characterizing equation (26). It is therefore appropriate to consider the equation of motion of the phase field ρ^N.

Unlike numerical segregation (or recoloring) strategies [8], a formulaic segregation method is amenable to analysis. To facilitate this analysis we describe formulaic segregation formally using a single relaxation time LBGK evolution equation with collision parameter ω_c and we obtain the corresponding macroscopic dynamics by a Chapman-Enskog expansion process. The segregation encapsulated in Eq. (26) represents a special case of the following, generalized formulaic segregation or "color collision":

$$R_i(\mathbf{r}+\mathbf{c}_i,t+1)=R_i(\mathbf{r},t)-\omega_c[R_i(\mathbf{r},t)-R_i^{(0)}], \tag{43}$$

with

$$R_i^{(0)}\equiv\frac{R}{R+B}f_i^{\dagger}(\mathbf{r},t)+\beta\left(\frac{1}{R}+\frac{1}{B}\right)^{-1}t_p\cos[\theta_f(\mathbf{r},t)-\theta_i]|\mathbf{c}_i|, \tag{44}$$

in which $R=R(\mathbf{r},t)$. We emphasize that Eq. (44) is a generalized segregation; setting $\omega_c=1$ will enable us to extract the macroscopic dynamics of the particular formulaic segregation after Refs. [13,14]; it is not our aim here to consider a generalized segregation process. Note that we have reexpressed the bracket term in the last equation and that $f_i^{\dagger}$ includes any source term contribution [see Eq. (21)].

We assume that it is possible to expand the $R_i(\mathbf{r},t)$ about equilibrium

$$R_i(\mathbf{r},t)=\sum_n \epsilon^n R_i^{(n)}, \tag{45}$$

where ϵ is a Chapman-Enskog parameter. It is now straightforward to obtain the following three results for the moments of $R_i^{(0)}$. First,

$$\sum_i R_i^{(0)}=R(\mathbf{r},t)\equiv\sum_i R_i(\mathbf{r},t), \tag{46}$$

$$\sum_i R_i^{(0)}\mathbf{c}_i=R\mathbf{u}^*+k_2\beta\left(\frac{1}{R}+\frac{1}{B}\right)^{-1}\hat{\mathbf{f}}'+f\frac{R}{R+B}\mathbf{F}\equiv\mathbf{q}_R^{\dagger\dagger}, \tag{47}$$

$$\sum_i R_i^{(0)}c_{i\alpha}c_{i\beta}=\frac{R}{R+B}\sum_i f_i^{\dagger}c_{i\alpha}c_{i\beta}\equiv\Lambda_{R\alpha\beta}, \tag{48}$$

where we have used Eq. (29) and, in the third (last) equation, we have used the fact that odd moments of the lattice are zero. We define

$$\Lambda_{\alpha\beta}\equiv\Lambda_{R\alpha\beta}-\Lambda_{B\alpha\beta}. \tag{49}$$

We shall use equations (47)–(49) shortly. For the moment, note that Eq. (46) implies that

$$\sum_i R_i^{(n>1)}=0, \tag{50}$$

but, note, we cannot infer a corresponding result for the first moment of the $R_i^{(0)}$: $\Sigma_i R_i^{(n>1)}c_{i\alpha}\neq 0$. From Eqs. (43)–(50), only Eq. (47) changes under the exchange $B\leftrightarrow R$ as follows:

$$\sum_i B_i^{(0)}\mathbf{c}_i=B\mathbf{u}^*-k_2\beta\left(\frac{1}{R}+\frac{1}{B}\right)^{-1}\hat{\mathbf{f}}'+f\frac{B}{R+B}\mathbf{F}\equiv\mathbf{q}_B^{\dagger\dagger}, \tag{51}$$

and so

$$\sum_i (R_i^{(0)}-B_i^{(0)})\mathbf{c}_i=\rho\rho^N\mathbf{u}^*+2k_2\beta\left(\frac{1}{R}+\frac{1}{B}\right)^{-1}\hat{\mathbf{f}}'+f\rho^N\mathbf{F}=\mathbf{q}^{\dagger\dagger}, \tag{52}$$

where, in the second part of the equality, we have used Eq. (32).

Now, we proceed in the usual fashion; that is, by using a Taylor expansion of the evolution equation (43) about $\mathbf{r}$, t and a subsequent expansion of (only) the time derivative [1] as follows:

$$\partial_t=\partial_{t0}+\epsilon\partial_{t1},\quad \partial_x=\epsilon\partial_x, \tag{53}$$

as discussed in Refs. [1] and [17]. The Chapman-Enskog expansion then generates the following equations. At $o(\epsilon)$,

$$\partial_{t0}R_i^{(0)}+c_{i\alpha}\partial_\alpha R_i^{(0)}=-\omega_c R_i^{(1)}, \tag{54}$$

and at $o(\epsilon^2)$,

$$\partial_{t1}R_i^{(0)}+\left(1-\frac{\omega_c}{2}\right)(\partial_{t_0}+c_{i\alpha}\partial_\alpha)R_1^{(1)}=-\omega_c R_i^{(2)}. \tag{55}$$

Let us consider the $o(\epsilon)$ dynamics. Summing Eq. (54) over i, using Eq. (50) and definition (47), we obtain

$$\partial_{t0}R+\boldsymbol{\nabla}\cdot\left(R\mathbf{u}^*+k_2\beta\left[\frac{1}{R}+\frac{1}{B}\right]^{-1}\hat{\mathbf{f}}'+f\frac{R}{R+B}\mathbf{F}\right)=0, \tag{56}$$

and similarly, for the quantity B,

$$\partial_{t0}B+\boldsymbol{\nabla}\cdot\left(B\mathbf{u}^*-k_2\beta\left[\frac{1}{R}+\frac{1}{B}\right]^{-1}\hat{\mathbf{f}}'+f\frac{B}{R+B}\mathbf{F}\right)=0. \tag{57}$$

Subtracting Eqs. (56) and (57), there results the following macroscopic dynamics for the phase field scalar at $o(\epsilon)$:

$$\partial_{t0}\rho\rho^N+\partial_\alpha\rho\rho^N u_\alpha^*=-2k_2\beta\partial_\alpha\left(\left[\frac{1}{R}+\frac{1}{B}\right]^{-1}\hat{f}'_\alpha\right)-f\partial_\alpha(\rho^N F_\alpha). \tag{58}$$

Multiply Eq. (54) by link velocity component $c_{i\beta}$, sum the resulting equation over i, and follow a similar analysis to obtain [still at $o(\epsilon)$]

$$\partial_{t0}\left(\rho\rho^N u_\beta^*+2k_2\beta\left(\frac{1}{R}+\frac{1}{B}\right)^{-1}\hat{f}'_\beta+f\rho^N F_\beta\right)+\partial_\alpha\Lambda_{\alpha\beta}=-\omega_c\sum_i (R_i^{(1)}-B_i^{(1)})c_{i\beta}, \tag{59}$$

and in the expression in the right-hand side approximate $C_i^{(1)}\approx(C_i-C_i^{(0)})$ $(C=R,B)$ and use Eqs. (25) and (52); Eq. (59) now becomes

$$\partial_{t0}\left(\rho\rho^N\mathbf{u}^*+2k_2\beta\left(\frac{1}{R}+\frac{1}{B}\right)^{-1}\hat{\mathbf{f}}'+f\rho^N\mathbf{F}\right)+\partial_\beta\Lambda_{\alpha\beta}=\omega_c(\mathbf{q}^{\dagger\dagger}-\mathbf{q}). \tag{60}$$

Next consider the $o(\epsilon^2)$ dynamics. In Eq. (55), substitute for $R_i^{(1)}$ from Eq. (54) and again sum on i; after some algebra, we obtain

$$\partial_{t1}R + \left(\frac{1}{2} - \frac{1}{\omega_c}\right)\left(\partial_{t0}^2 R + 2\partial_{t0}\partial_\alpha\left(\sum_i R_i^{(0)} c_{i\alpha}\right) + \partial_\alpha\partial_\beta\Lambda_{R\alpha\beta}\right) = 0, \tag{61}$$

with a corresponding equation for B, which, when subtracted from Eq. (61), yields

$$\partial_{t1}\rho\rho^N + \left(\frac{1}{2} - \frac{1}{\omega_c}\right)\left\{\partial_{t0}^2\rho\rho^N + 2\partial_{t0}\partial_\alpha\left[\rho\rho^N u_\alpha^* + 2k_2\beta\left(\frac{1}{R} + \frac{1}{B}\right)^{-1}\hat{f}'_\alpha + f\rho^N F_\alpha\right] + \partial_\alpha\partial_\beta\Lambda_{\alpha\beta}\right\} = 0, \tag{62}$$

where we have used Eq. (52). By using Eqs. (60) and (58) it is possible, again after some algebra, to obtain from the last equation the following dynamics for the phase field at $o(\epsilon^2)$:

$$\partial_{t1}\rho\rho^N = \left(1 - \frac{\omega_c}{2}\right)\nabla\cdot(\mathbf{q}^{\dagger\dagger} - \mathbf{q}). \tag{63}$$

In Appendix B we obtain an expression for the color flux $\mathbf{q}$; from this expression, we now retain only the first order in gradient quantities as follows:

$$q_\alpha = \rho\rho^N u_\alpha^* - c_s^2\partial_\alpha(\rho\rho^N) + f\rho^N F_\alpha + \frac{1}{2}\frac{\beta}{k}k_2\rho\partial_\alpha\rho^N, \tag{64}$$

which, when combined with Eq. (37), allows us to reexpress the right-hand side of Eq. (63) to obtain

$$\partial_{t1}\rho\rho^N = \frac{1}{2}c_s^2\nabla^2(\rho\rho^N), \tag{65}$$

in which equation we have now set $\omega_c=1$ and used the fact that $k=\beta$. To combine the $o(\epsilon)$ and $o(\epsilon^2)$ time scales, add Eqs. (58) and (ϵ times) (65), invoke identity (53), and use the facts that $k=\beta$ and, in LBGK models, $k_2=c_s^2$ [17],

$$\partial_t\rho\rho^N + \nabla\cdot(\rho\rho^N\mathbf{u}^*) = -f\nabla\cdot(\rho^N\mathbf{F}) + \frac{1}{2}c_s^2\nabla\cdot(\rho^N\nabla\rho). \tag{66}$$

Now, Eq. (66) describes the behavior of the phase field for the multicomponent LBGK model based upon Guo's enhanced variant ($f=1/2$) and for the standard, unmodified model ($f=1$). We proceed to consider the final form of the phase-field dynamics for these two cases, separately.

Consider Guo's LBGK model, characterized by $f=1/2$. On utilizing the continuity equation (18a) of Ref. [10], for the lattice fluid

$$\partial_t\rho + \nabla\cdot(\rho\mathbf{u}^*) = 0, \tag{67}$$

it is straightforward to manipulate Eq. (66) into a form containing the material derivative

$$\frac{d}{dt}\rho^N = \frac{1}{2\rho}\nabla\cdot(c_s^2\rho^N\nabla\rho - \rho^N\mathbf{F}), \tag{68}$$

where, note, interface force $\mathbf{F}$ [see Eq. (10) and associated discussion] is impressed on the fluid only in the interfacial region.

For the standard LBGK model, it is possible to show that the presence of a variable fluid body force $\mathbf{F}$ generates additional terms in the lattice fluid continuity equation for the lattice fluid [20,21], which becomes

$$\partial_t\rho + \nabla\cdot(\rho\mathbf{u}) = -\frac{1}{2}\nabla\mathbf{F}, \tag{69}$$

which now implies phase-field dynamics as follows:

$$\frac{d}{dt}\rho^N = -\frac{1}{2\rho}\nabla\cdot(\rho^N\mathbf{F}) + \rho^N\frac{1}{2\rho}\nabla\cdot(\mathbf{F}) = -\frac{1}{2\rho}\mathbf{F}\cdot\nabla\rho^N. \tag{70}$$

In a continuum fluid, the interface is subject to a kinematic condition, which requires that it (the interface) move at the same speed as the local fluids. For a point in the interface, identified by a chosen value of ρ^N, to advect with local flow requires a condition $\frac{d\rho^N}{dt}=0$. It follows that, in either of the models (and, indeed, in all multicomponent lB) the interface is accelerated relative to the local fluid, in fact by an amount independent of the local flow and interfacial tension, determined mainly by local phase-field gradients. Qualitatively at least, these observations accord with the observations of Latva-Kokko and Rothman [14]. Approximating ρ =constant, the value of ρ^N, and hence the term in the right-hand side of each of the equations, clearly varies across the interfacial region indicating unphysical, relative movement between the phase field and the lattice fluid in both models.

To restore this lack of a kinematic condition we attempt to limit the differential motion of the lattice fluid and the phase field on closed contour $\rho^N=0$; the latter appears to the authors to be the lattice region onto which efforts (algorithmic extensions) designed more strongly to promote a kinematic condition are best concentrated. None of the several flavors of the lB interface strategies currently in use explicitly impose a kinematic condition. In the associated article [19] we address the issue of simple, portable, and effective kinematic condition, independent of the background interface model.

IV. RESULTS

Reduction in the pinning of advected drops, resulting from the use of this recoloring strategy, has been reported by Latva-Kokko and Rothman [14] elsewhere. While the latter uses a different multicomponent lB model (the surface-tension generating algorithm of Gunstensen [8] is used), Latva-Koko and Rothman effectively demonstrate that it is the recoloring or segregation steps, which lie at the root of an improvement in drop advection, or Galilean invariance properties. Not surprisingly, very similar improvements were observed with our particular lB model and we proceed to report, in this section, other improvements associated with

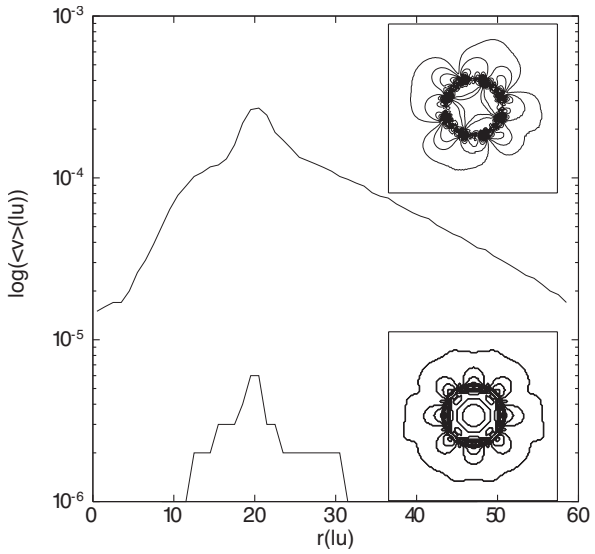

FIG. 5. Average interfacial microcurrent activity $\langle v \rangle$ measured in lattice units, plotted as a function of radial distance from the drop center r measured in lattice units, for numerical segregation (upper curve) and for the distributed segregation method (lower curve) for otherwise identical drops. Note the use of the logarithmic scale on the ordinate. There is a difference of almost two orders of magnitude in the microcurrent activity.

macroscopic fluid-interfacial properties of the model, which accrue from the use of a fomulaic segregation procedure.

Use of the segregation of Sec. III is, alone, responsible for a considerable reduction in the unphysical spurious velocity activity (or interfacial microcurrent), created by the interface. Microcurrent activity was measured as follows. An equilibrated drop of initial radius 20 lattice units was placed on a square lattice, bounded using a second-order accurate boundary closure [18] for no-slip conditions. The measured velocity modulus was averaged over annular lattice samples of increasing average radius, centered on the drop center of mass. We denote this activity average A. This procedure was performed on otherwise identical drops (surface tension parameter and the interfacial pressure steps) maintained (i) by numerical component segregation [8] and (ii) by the formulaic segregation method of Sec. III. Figure 5 shows the value of A as a function of distance from the drop center, for (upper line) the numerical and (lower line) the formulaic segregation method. Note the use of a logarithmic ordinal scale. The figure insets show the corresponding steady-state microcurrent flow fields, by means of a stream function plot.

For $\beta < 0.71$, stable interface profiles were found to be smooth and well approximated by a variation $\rho^N = \tanh(ks)$ with s distance in the direction of $\nabla\rho^N$ and $k=\beta$, the segregation parameter introduced in Eq. (26) (see Fig. 2). This fact, together with the smooth variation of ρ^N, encourages one to seek a local expression for the gradient in ρ^N, the existence of which would make the algorithm entirely local and very efficient.

It is possible to derive a local expression for $\nabla\rho^N$, which was found to work poorly for highly curved (or small) drops but surprisingly well for drops with curvature $K < 0.1$. We give a derivation in Appendix C. Figure 7 shows the key property of phase-field gradient for a circular (drop) interface, initial radius 20 lattice units, simulated by using these local approximations derived in Appendix C. Only lattice sites with both red and blue fluids present have a defined interfacial normal and phase-field gradient in Fig. 7. Note that the peak value of $\nabla\rho^N$ corresponds to $\rho^N = 0$.

In Appendix D, we present a brief note on the generalization of D'Ortona's segregation rule, to lB models for situations where more than two, mutually immiscible, continuum fluids are present [3].

V. CONCLUSION

We have presented a multicomponent lattice Boltzmann simulation applied in the continuum approximation of fluid mechanics, to completely immiscible fluids, paying particular attention to the component segregation part of the underlying algorithm. The principal practical outcome of this paper is the result that the overall algorithm is found to produce a very low level of microcurrent activity indeed; the principal methodological result of this paper is the derivation of the dynamics of a component index, or phase field, which have here been obtained for the formulaic segregation method of d'Ortona *et al.* [13] and Latva-Kokko and Rothman [14], using the method of Chapman-Enskog analysis. The dynamics accord with a simulation designed to address multicomponent flow in the continuum approximation and provide greatly improved simulation performance is as follows.

The segregation method analyzed has been shown to produce a very marked reduction in the interfacial microcurrent activity associated with a curved interface, which makes the method valuable (i) in terms of the improved quality of its results and (ii) by facilitating simulational access to regimes of flow with a low capillary number and drop Reynolds number [11]. While it (the formulaic segregation method) produces an interface which is distributed in terms of its component index, the hydrodynamic boundary conditions which it enforces (when used in conjunction with Lishchuk's method [9]) support the notion of a sharp, unstructured, continuum interface as effectively as other lB methods. Furthermore, it is possible to use further algorithmic extensions with the model discussed here to improve performance in this respect [19].

For continuum applications, we find that, in addition to improved hydrodynamic properties, a formulaic segregation method is considerably more computationally efficient than other methods (e.g., numerical segregation), especially when used with a locally calculated interface normal, which the method is able to support under certain circumstances. In the related paper [19] we set out to demonstrate an additional degree of flexibility associated with a formulaic segregation method, which may be exploited further to improve the accuracy of multiple component simulation with lattice Boltzmann.

APPENDIX A: PHASE-FIELD SOLUTION FOR A FLAT INTERFACE

Latva-Kokko and Rothman derive a form for a flat interface profile; we perform a similar analysis in this section,

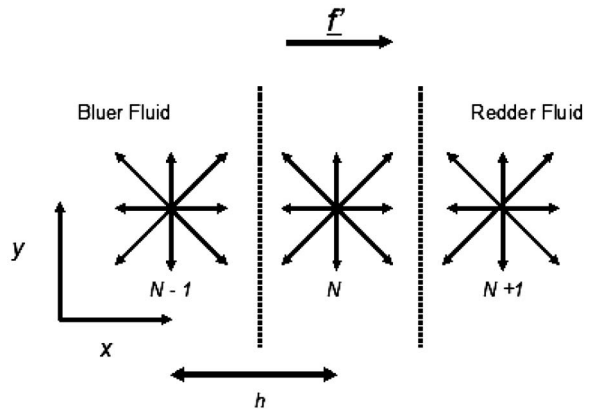

FIG. 6. Analysis of a flat, equilibrium interface orientated perpendicular to short lattice links. The lattice links on each of the nodes depicted are indexed as in Fig. 1. The color gradient points from left to right; the vertical broken lines represent contours of constant phase-field value.

making comparisons with Ref. [14] where appropriate. Consider a lattice fluid a rest with uniform density ρ, in the steady state, containing a flat interface parallel to short lattice links in a D2Q9 fluid. This situation is depicted in Fig. 6, in which two contours of constant phase-field parameter ρ^N are represented by broken lines and three adjacent lattice sites are shown. The indexing of the link label i for all three sites is as defined in Fig. 1. Note that an explicit lattice spacing h parameter has been introduced for present purposes.

The color gradient field unit vector $\hat{f}' = \hat{x}$. For the situation depicted in Fig. 6 there is no variation of ρ^N with the y coordinate; furthermore, on grounds of symmetry alone,

$$R_3(x_n,y) = R_5(x_n,y), \quad R_1(x_n,y) = R_8(x_n,y),$$
$$R_2(x_n,y) = R_6(x_n,y), \tag{A1}$$

where R may be a precollision or postcollision value and $n=(N-1),N,(N+1)$.

At equilibrium, there is no change of color content at any site and, henceforth, suppressing the y coordinate, we can write the following equilibrium condition for the red density on site N:

$$R(x_N) = 2R_3^{\dagger\dagger}(x_{N-1}) + R_4^{\dagger\dagger}(x_{N-1}) + 2R_2^{\dagger\dagger}(x_N) + 2R_1^{\dagger\dagger}(x_{N+1}) + R_8^{\dagger\dagger}(x_{N+1}) + R_0^{\dagger\dagger}(xN). \tag{A2}$$

Using Eq. (38) for $R_i^{\dagger\dagger}$ with the equilibrium solution $f_i^{\dagger} = t_p\rho$ with appropriate values of t_p and color field $\hat{f}$, the last equation may, after some simple algebra, be written as

$$2R(x_N) = R(x_{N-1})\{1 + \beta'[\rho - R(x_{N-1})]\} + R(x_{N+1})\{1 - \beta'[\rho - R(x_{N+1})]\}, \tag{A3}$$

where $\beta' = \beta/\rho$. Taylor expanding the terms in this equation about x_N, to second order in lattice parameter h, it is straightforward to obtain the following equation for the red density $R(x)$ at equilibrium:

$$\frac{d^2R}{dx^2} - 2\frac{\beta}{h}\frac{dR}{dx} + 2\frac{\beta'}{h}\frac{dR^2}{dx} = 0, \tag{A4}$$

which may be integrated once, straightforwardly to obtain a separable first-order differential equation as follows:

$$\frac{dR}{dx} = \frac{2\beta}{h}R\left(1 - \frac{R}{\rho}\right), \tag{A5}$$

which, note, differs only superficially from Eq. (15) of Latva-Kokko and Rothman [14]. The last equation may be readily integrated. On supposing that the site at x_N lies at the center of an interface, the constants of integration are easily obtained as follows:

$$R(x) = \frac{\rho}{2}\left(\tanh\left(\frac{\beta}{h}(x - x_N)\right)\right), \tag{A6}$$

as is readily checked by substitution into Eq. (A4).

On setting $h=1$, segregation parameter β is seen to be the parameter of the equilibrium interface width; the result to which we appeal in Sec. III A. Clearly, the preceding analysis generalizes directly to the case of a 3D lattice.

For a D2Q9 lattice, a conceptually identical but somewhat more complicated analysis of the case of an interface parallel to the long links of the lattice shows that the equilibrium state of the interfacial phase field is described by differential equation (A4) solution (A6).

APPENDIX B: AN EXPRESSION FOR THE COLOR FLUX VECTOR

In this section we derive an expression for color flux vector (q). Substitute Eq. (24) into definition (25) and reverse the propagate step to obtain

$$\mathbf{q}(\mathbf{r},t) = \sum_i [R_i^{\dagger\dagger}(\mathbf{r} - \mathbf{c}_i, t-1) - B_i^{\dagger\dagger}(\mathbf{r} - \mathbf{c}_i, t-1)]\mathbf{c}_i. \tag{B1}$$

Substituting with Eq. (38) we obtain straightforwardly,

$$q_\alpha(\mathbf{r},t) = \sum_i \rho^N(\mathbf{r} - \mathbf{c}_i, t-1) f_i^{\dagger}(\mathbf{r} - \mathbf{c}_i, t-1) c_{i\alpha} + \frac{\beta}{2}\sum_i t_p\rho(\mathbf{r} - \mathbf{c}_i, t-1)[1 - \rho^N(\mathbf{r} - \mathbf{c}_i, t-1)^2]\hat{f}_\beta(\mathbf{r} - \mathbf{c}_i, t-1)c_{i\alpha}c_{i\beta}, \tag{B2}$$

in which, $f_i^{\dagger}$ contains the body-force source term contribution. We shall treat Eq. (B2) term by term. Note that we have used Eqs. (17) and (18) to set the second term on the right-hand side into the above form.

In continuum applications, the interfacial phase field is always close to equilibrium; accordingly we shall neglect its time variation. Moreover, bearing in mind the form of Eq. (70), it is necessary to work only to first order in space derivatives. Accordingly, the first term in the right-hand side of Eq. (B2) is treated by Taylor expanding $f_i^{\dagger\dagger}$ about $\mathbf{r}$, to obtain the following expression:

$$\rho^N\left(\sum_i f_i^\dagger c_{i\beta}\right) - \rho^N \partial_\alpha\left(\sum_i f_i^\dagger c_{i\alpha}c_{i\beta}\right) - (\partial_\alpha \rho^N)\sum_i f_i^\dagger c_{i\alpha}c_{i\beta} + o(\nabla^3). \tag{B3}$$

In Sec. III, Eq. (22) we showed that $\Sigma_i f^\dagger c_{i\alpha} = \rho u_\alpha^* + f F_\alpha$, with $f = 1, \frac{1}{2}$ for the standard and Guo variants, respectively. Expressions in macroscopic quantities for the second and third terms in expression (B3) may be obtained in like manner for the Guo variant: substitute for $f_i^\dagger$ using definition (21), replace f_i with $(f_i^{(0)} + \epsilon f_i^{(1)} + \cdots)$ then substitute using Eqs. (5), (9a), and (17) of Guo *et al.* [10], with Guo's time-step parameter $\Delta t = 1$ to obtain

$$\sum_i f_i^\dagger c_{i\alpha\beta} = c_s^2 \rho \delta_{\alpha\beta} + \rho u_\alpha^* u_\beta^* + \frac{1}{2}(u_\alpha^* F_\beta + u_\beta F_\alpha) + 2\left(1 - \frac{1}{\omega}\right) c_s^2 \rho S_{\alpha\beta}^*. \tag{B4}$$

For the standard model the equivalent result is well known.

$$\sum_i f_i^\dagger c_{i\alpha\beta} = c_s^2 \rho \delta_{\alpha\beta} + \rho u_\alpha u_\beta + F_\beta. \tag{B5}$$

The second term in the right-hand side of Eq. (B2) is first transformed using (i) Eq. (36) to replace the factor $[1-\rho^N(\mathbf{r}-\mathbf{c}_i, t-1)^2]$ with $|\nabla \rho^N|/k$ evaluated at position $\mathbf{r} - \mathbf{c}_i$ and (ii) the definition of $\widehat{f'_\beta}$, in Eq. (12). Thereafter, Taylor expansion and appeal to Eqs. (19) and (20) yields

$$\frac{1}{2}\frac{\beta}{k} k_2 \rho \partial_\alpha \rho^N + o(\nabla^3), \tag{B6}$$

where, recall $k = \beta$.

Using expressions (B3), (B6), Eqs. (B2) and (B4) it is possible to obtain, correct to first-order spatial gradients, the following expression for q_α in the Guo model:

$$q_\alpha(\mathbf{r},t) = \rho\rho^N u_\alpha^* - c_s^2 \partial_\alpha(\rho\rho^N) + \frac{1}{2}\rho^N F_\alpha + \frac{1}{2}\frac{\beta}{k} k_2 \rho \partial_\alpha \rho^N - \partial_\beta(\rho\rho^N u_\alpha^* u_\beta^*) - \frac{1}{2}\partial_\beta(\rho^N[u_\alpha^* F_\beta + u_\beta^* F_\alpha]) - 2\left(1 - \frac{1}{\omega}\right) c_s^2 \partial_\beta(\rho^N S_{\alpha\beta}), \tag{B7}$$

in which the terms in the second line are neglected. The corresponding result for the standard model is easily established using equations, again from expressions (B3), (B6), Eq. (B2), and now, Eq. (B5),

$$q_\alpha(\mathbf{r},t) = \rho\rho^N u_\alpha - c_s^2 \partial_\alpha(\rho\rho^N) + \rho^N F_\alpha \partial_\alpha \rho^N + \frac{1}{2}\frac{\beta}{k} k_2 \rho \partial_\alpha \rho^N. \tag{B8}$$

APPENDIX C: A LOCAL EXPRESSION FOR COLOR GRADIENT

We introduce in this section a local expression for $\mathbf{f}'(\mathbf{r})$, which provides a computationally efficient expression suitable for use with a formulaic segregation rule [expressed in Eqs. (26) and (38)] when the local interfacial curvature is not too great or changing too fast (see the discussion at the end of this Appendix).

For red and blue fluids define a local *color field*,

$$\mathbf{g}'(\mathbf{r},t) \equiv -\sum_i [R_i(\mathbf{r},t) - B_i(\mathbf{r},t)]\mathbf{c}_i, \tag{C1}$$

in which red and blue densities are precollision values. If propagation is taken to be instantaneous, it follows that $R_i(\mathbf{r},t) = R_i^{\dagger\dagger}(\mathbf{r}-\mathbf{c}_i, t-1)$ [and also that $f_i(\mathbf{r},t) = f_i^\dagger(\mathbf{r}-\mathbf{c}_i, t-1)$], accordingly,

$$\mathbf{g}'(\mathbf{r},t) \equiv -\sum_i [R_i^{\dagger\dagger}(\mathbf{r}-\mathbf{c}_i, t-1) - B_i^{\dagger\dagger}(\mathbf{r}-\mathbf{c}_i, t-1)]\mathbf{c}_i. \tag{C2}$$

Substitute from Eq. (26) into Eq. (C2) and use the identities (17) and (18) to obtain

$$\mathbf{g}'(\mathbf{r},t)_\alpha = S_\alpha^{(1)} + S_\alpha^{(2)}, \tag{C3}$$

where

$$S_\alpha^{(1)} = -\sum_i \rho^N(\mathbf{r}-\mathbf{c}_i, t-1) f_i(\mathbf{r},t) c_{i\alpha}, \tag{C4}$$

in which we have used the fact that $f_i^\dagger(\mathbf{r}-\mathbf{c}_i, t-1) = f_i(\mathbf{r},t)$ and

$$S_\alpha^{(2)} = -\frac{\beta}{2}\sum_i t_p \rho(\mathbf{r}-\mathbf{c}_i, t-1)[1 - (\rho^N(\mathbf{r}-\mathbf{c}_i, t-1))^2] \times \cos(\theta_g(\mathbf{r}-\mathbf{c}_i, t-1) - \theta_i) c_{i\alpha}, \tag{C5}$$

in which $\theta_g(\mathbf{r})$ is the direction of the color field. Using the approximation in Eq. (36), Eq. (C5) may be transformed as follows:

$$S_\alpha^{(2)} = -\frac{\beta}{2k}\sum_i t_p \rho(\mathbf{r}-\mathbf{c}_i, t-1) \times (\partial_x \rho^N|_{\mathbf{r}-\mathbf{c}_i, t-1} c_{ix} c_{i\alpha} + \partial_y \rho^N|_{\mathbf{r}-\mathbf{c}_i, t-1} c_{iy} c_{i\alpha}). \tag{C6}$$

.

Henceforth neglect explicit time dependence. Noting that both Eqs. (C6) and (C4) remain true in D3QN, we proceed by expanding the right-hand side of both [Eqs. (C6) and (C4)] about $\mathbf{r}$ and, using the expressions (19) and (20) for second and fourth moments of the lattice vectors, we obtain, after some algebra,

$$S_\alpha^{(1)} = -\rho^N(\mathbf{r})\rho(\mathbf{r})u_\alpha^* + \partial_\beta \rho^N(\mathbf{r}) \sum_i f_i(\mathbf{r}) c_{i\alpha} c_{i\beta}, \tag{C7}$$

$$S_\alpha^{(2)} = -\frac{\beta}{2k} k_2 \rho(\mathbf{r}) \partial_\alpha \rho^N(\mathbf{r}) - \frac{\beta}{2k} k_4 \{\partial_\alpha \rho(\mathbf{r}) \nabla^2 \rho^N(\mathbf{r}) + 2\partial_\theta \rho(\mathbf{r}) \partial_\alpha \partial_\theta \rho^N(\mathbf{r})\}. \tag{C8}$$

The quantity $\Sigma_i f_i(\mathbf{r}) c_{i\alpha} c_{i\beta}$ in Eq. (C7) may be replaced by the sum of the zeroth and first-order momentum flux (stress) tensors; wishing only to retain terms linear in gradient quantities we make the approximation

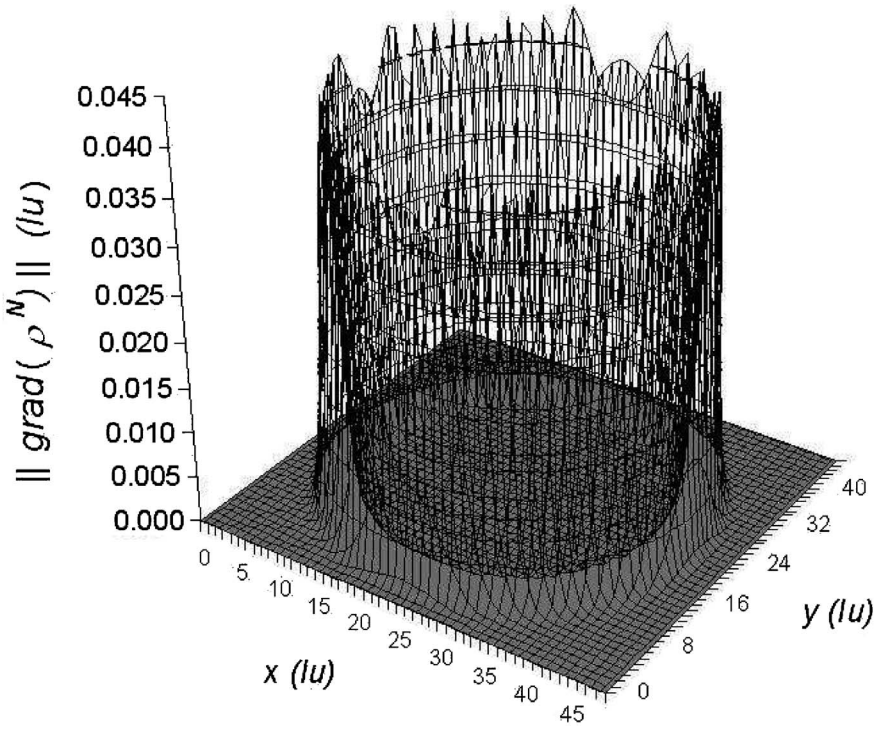

FIG. 7. Variation of the phase-field gradient for a red drop immersed in a blue fluid (z axis) versus position. $\nabla\rho^N$ (z axis) was calculated using the local approximation, given in Eq. (C12), derived in Appendix C. The drop initial radius was 20 lattice units. Only lattice sites with both red and blue fluids present have a defined interfacial phase-field gradient. Note that the peak value of $\nabla\rho^N$ corresponds to $\rho^N=0$.

$$\sum_i f_i(\mathbf{r})c_{i\alpha}c_{i\beta} \approx \sum_i f_i^{(0)}(\mathbf{r})c_{i\alpha}c_{i\beta} = c_s^2\rho + \rho u_\alpha^* u_\beta^*, \quad \text{(C9)}$$

where c_s is the speed of sound. We may now approximate Eqs. (C7) and (C8) as follows:

$$S_\alpha^{(1)} \simeq -\rho^N(\mathbf{r})\rho(\mathbf{r})u_\alpha^* + c_s^2\rho(\mathbf{r})\partial_\alpha\rho^N(\mathbf{r}), \quad \text{(C10)}$$

$$S_\alpha^{(2)} = -\frac{\beta}{2k}k_2\rho(\mathbf{r})\partial_\alpha\rho^N(\mathbf{r}). \quad \text{(C11)}$$

Equation (C3) now yields the following local approximation to the color gradient:

$$\nabla\rho^N(\mathbf{r}) = \frac{1}{A}[\mathbf{g}' + \rho(\mathbf{r})\rho^N(\mathbf{r})\mathbf{u}^*], \quad A \equiv \rho(\mathbf{r})\left(c_s^2 - \frac{\beta}{2k}k_2\right). \quad \text{(C12)}$$

From simulations in D2Q9, for which $c_s^2=1/3$, with segregation parameter $\beta=0.7$, $\rho(\mathbf{r})=2$, we measure $1/A=2.37$, compared with a calculated value of 3.14. While use of the above expression is found to produce instabilities when the local interfacial curvature $K>0.1$, it does underwrite a useful increase in the execution speed, determined, of course, by the total amount of interface in the simulation. For a drop of initial radius 20 lattice units, Fig. 7 shows a surface plot of the value of $\nabla\rho^N(\mathbf{r})$ measured using Eq. (C12).

APPENDIX D: GENERALIZATION OF METHOD TO $N>2$ MUTUALLY IMMISCIBLE FLUID COMPONENTS

Lattice Boltzmann models of multiple, mutually immiscible, continuum fluids have been successfully applied in the simulation of microfluidic devices [2]; in this section we consider how a formulaic segregation method after d'Ortona and Latva-Kokko may be applied to the model used in Ref. [2] and first presented in Ref. [3].

Any attempt to generalize Eq. (26) to multiple immiscible fluids is complicated (i) by the definition of appropriate phase or color fields to guide the segregation and (ii) by the weight factor of the (second right-hand side) segregation term of Eq. (26).

Let us consider three mutually immiscible fluids, designated red (nodal mass R), blue (nodal mass B), and green (nodal mass G). Let C and C' denote two colors in general. All notation is extended from that used earlier in this paper.

We introduce a *two-component* local color field, which may be defined between all colors C and C'. We choose to define this in local terms; the following discussions are, of course, valid for a nonlocal equivalent as follows:

$$f_\alpha^{CC'} = -\sum_i [f_i^{C'}(\mathbf{r}) - f_i^C(\mathbf{r})]c_{i\alpha}, \quad \text{(D1)}$$

which has the property that $f_\alpha^{CC'} = -f_\alpha^{C'C}$ or, in terms of angles,

$$\theta^{CC'} = \theta^{C'C} + \pi. \quad \text{(D2)}$$

For three colors $C=R,B,G$ the $3!/2$ possible two-component local color fields are $\mathbf{f}^{RB}$, $\mathbf{f}^{RG}$, $\mathbf{f}^{BG}$. Noting that what follows remains valid for the nonlocal equivalent of the definition in Eq. (D1) we now propose a generalization of formulaic segregation in Eq. (26) as follows:

$$R_i^{\dagger\dagger} = \frac{R}{\rho} f_i^{\dagger} + \frac{R}{\rho}[\beta_{RB} B \cos(\theta^{RB} - \theta_i) + \beta_{RG} G \cos(\theta^{RG} - \theta_i)|\mathbf{c}_i|], \tag{D3}$$

where we have used $\rho=(R+B+G)$. Note that it is essential to have $\beta_{RB}=\beta_{BR}$ but $\beta_{RC} \neq \beta_{BC'}$ necessarily. In general, the segregation of Eq. (D3) is

$$f_i^{C\dagger\dagger} = \frac{C}{\rho}\left(f_i^{\dagger} + \sum_{C' \neq C} \beta_{CC'} C' \cos(\theta^{CC'} - \theta_i)|\mathbf{c}_i|\right), \tag{D4}$$

where the summation runs over all the $N_c(\mathbf{r})$ colors on the node at $\mathbf{r}$. With $\beta^{CC'}=\beta$, Eq. (D4) reduces to

$$f_i^{C\dagger\dagger} = \frac{C}{\rho}\left(f_i^{\dagger} + \beta \sum_{C' \neq C} C' \cos(\theta^{CC'} - \theta_i)|\mathbf{c}_i|\right). \tag{D5}$$

On taking the summation over C we now observe the desired properties

$$\sum_C f_i^{C\dagger\dagger} = f_i^{\dagger} \frac{\sum_C C}{\rho} + \frac{\beta}{\rho}\left(\sum_{C,(C' \neq C)} CC' \cos(\theta^{CC'} - \theta_i)|\mathbf{c}_i|\right), \tag{D6}$$

for, on using Eq. (D2), terms in the summation cancel in pairs and

$$\sum_C f_i^{C\dagger\dagger} = f_i^{\dagger} \frac{\rho}{\rho} = f_i^{\dagger}. \tag{D7}$$

[1] S. Succi, *The lattice Boltzmann Equation for Fluid Dynamics and Beyond* (Clarendon, Oxford, 2001).
[2] M. M. Dupin, I. Halliday, and C. M. Care, Phys. Rev. E **73**, 055701(R) (2006).
[3] M. M. Dupin, I. Halliday, and C. M. Care, J. Phys. A **36**, 8517 (2003).
[4] M. M. Dupin, I. Halliday, and C. M. Care, Philos. Trans. R. Soc. London, Ser. A **362**, 1885 (2004).
[5] M. R. Swift, W. R. Osborn, and J. M. Yeomans, Phys. Rev. Lett. **75**, 830 (1995).
[6] X. W. Shan and H. D. Chen, Phys. Rev. E **49**, 2941 (1994).
[7] M. R. Swift, E. Orlandini, W. R. Osborn, and J. M. Yeomans, Phys. Rev. E **54**, 5041 (1996).
[8] A. K. Gunstensen, D. H. Rothman, S. Zaleski, and G. Zanetti, Phys. Rev. A **43**, 4320 (1991).
[9] S. V. Lishchuk, C. M. Care, and I. Halliday, Phys. Rev. E **67**, 036701 (2003).
[10] Z. Guo, C. Zheng, and B. Shi, Phys. Rev. E **65**, 046308 (2002).
[11] I. Halliday, R. Law, C. M. Care, and A. Hollis, Phys. Rev. E **73**, 056708 (2006).
[12] L. Landau and E. M. Lifshitz, *Fluid Mechanics*, 2nd ed. (Butterworth-Heinemann, 1987).
[13] U. D'Ortona, D. Salin, M. Cieplak, R. B. Rybka, and J. R. Banavar, Phys. Rev. E **51**, 3718 (1995).
[14] M. Latva-Kokko and D. H. Rothman, Phys. Rev. E **71**, 056702 (2005).
[15] Y. H. Qian, D. d'Humieres, and P. Lallemand, Europhys. Lett. **17**, 479 (1992).
[16] A. J. C. Ladd and R. Verberg, J. Stat. Phys. **104**, 1191 (2001).
[17] S. Hou, Q. Zou, S. Chen, G. Doolen, and A. C. Cogley, J. Comput. Phys. **118**, 329 (1995).
[18] A. Hollis and I. Halliday, J. Phys. A **39**, 10589 (2006).
[19] A. Hollis and I. Halliday, following paper, Phys. Rev. E **76**, 026709 (2007).
[20] I. Halliday, L. A. Hammond, C. M. Care, K. Good, and A. Stevens, Phys. Rev. E **64**, 011208 (2001).
[21] T. Reis and T. N. Phillips, Phys. Rev. E **75**, 056703 (2007).